Materials and Solidification

Research Article

Correlating melt structure, viscosity, and Ca content in Mg–Ca alloys via molecular dynamics

Dengyuan Qi[1], Ang Zhang[1,✉], Lijun Zhang[1], Tao Jiang[1], Feng He[2], Jun Wang[2], Zehua Li[1], Xiao Li[1], Jiangfeng Song[1], Bin Jiang[1,3]

Cite this article: Qi D, Zhang A, Zhang L, et al. *Materials and Solidification* 2026, **2**(1): 9580018. https://doi.org/10.26599/MAS.2026.9580018

ABSTRACT: As a key alloying element in magnesium (Mg) alloys, calcium (Ca) effectively enhances their oxidation resistance, high-temperature strength, and castability. However, experimentally determining the regulatory mechanism of Ca on the fluidity of Mg alloy melts remains challenging due to the high volatility and oxidation tendency of the alloy melts. To address this, molecular dynamics simulations are employed to systematically calculate the structural parameters (pair distribution function, coordination number, Voronoi index, and Honeycutt–Anderson index) and viscosity of Mg–Ca alloy melts across a Ca content range of 0.1–10 wt% (covering low concentrations to near the eutectic point of 10.5 wt%). At low Ca concentrations, the degree of structural order in the melt exhibits oscillatory changes with increasing Ca content (< 4 wt%), accompanied by significant structural fluctuations. In contrast, the structural order increases slightly with Ca content at high Ca concentrations (> 4 wt%), leading to enhanced structural stability. Throughout the entire Ca concentration range, ICO-type bonded pairs remain predominant, underscoring their critical role in maintaining the short-range ordered structure. As the Ca content increases, the atomic diffusion capability decreases, while the melt viscosity shows an overall increasing trend, with values calculated via both equilibrium molecular dynamics and nonequilibrium molecular dynamics methods confirming this trend. This study provides a microscopic theoretical basis for elucidating the regulatory mechanism of Ca on the fluidity of Mg–Ca alloy melts by establishing a quantitative correlation between Ca content, melt structure, and viscosity.

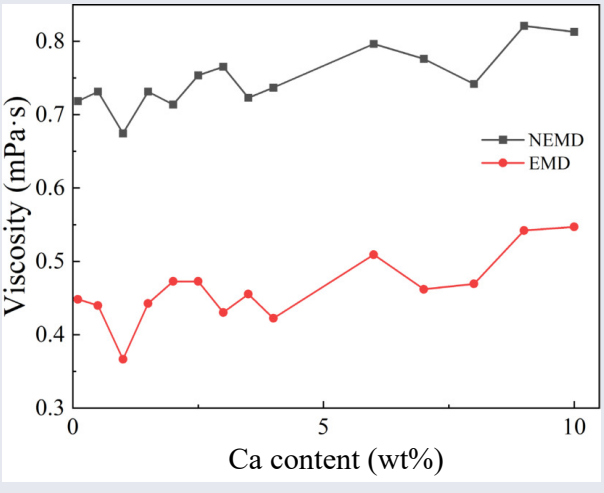

KEYWORDS: Mg alloys; melt structure; viscosity; molecular dynamics

1 Introduction

Magnesium alloys, as the lightest metallic structural materials, possess excellent specific strength, damping capacity, and electromagnetic shielding performance, granting them significant application potential in aerospace, new energy vehicles, and electronic devices [1–6]. Casting is a primary forming process for magnesium alloy components [7–10]. During casting, the fluidity of the alloy melt directly determines the mold-filling capability, which in turn impacts the quality of the formed component. Alloy melt fluidity is governed by the coupled effects of alloy properties, process parameters, and component geometry, among which viscosity is a core influencing factor. The value of the viscosity largely dictates the flow rate of the liquid metal during mold filling.

The viscosity reflects the atomic transport properties of the melt and is a structure-sensitive property of metal melts. Currently, understanding the evolution of complex atomic clusters in magnesium alloy melts and their correlation with temperature represents a forefront and challenging research area. Relying solely on empirical correlations of macroscopic fluidity parameters without elucidating their underlying structural origins leads to blindness in the prediction and control of fluidity. Therefore, precisely revealing the intrinsic relationship between melt structure and viscosity is key to advancing magnesium alloy casting from a traditional "trial-and-error" approach toward a

[1] National Engineering Research Center for Magnesium Alloys, National Key Laboratory of Advanced Casting Technologies, College of Materials Science and Engineering, Chongqing University, Chongqing 400044, China. [2] State Key Laboratory of Solidification Processing, Northwestern Polytechnical University, Xi'an 710072, China. [3] Institute of Lightweight Materials and Engineering, Mingyue Lake Laboratory, Chongqing 401122, China.

✉ Corresponding author. E-mail: angzhang@cqu.edu.cn

Received: November 14, 2025; Revised: December 25, 2025; Accepted: January 4, 2026

physics-based "rational design". This can provide theoretical support for the precise formation of high-performance, complex-structure magnesium alloy castings.

Calcium (Ca), as a low-cost and environmentally friendly alloying element, has attracted significant attention in the field of magnesium alloys in recent years. Studies have confirmed that the addition of Ca can significantly enhance the oxidation resistance, high-temperature strength, and castability of magnesium alloys [11]. A composite MgO–CaO protective film forms on the surface of Mg–Ca alloys, effectively improving oxidation resistance [12]. The hardness and tensile strength of Mg–Ca alloys increase with increasing Ca content [13]. Ca can also react with Al to form Al_2Ca phases in Mg–Al-based alloys, which suppresses the precipitation of the detrimental β-$Mg_{17}Al_{12}$ phase, thereby refining grains and improving corrosion resistance [14]. Moreover, in Mg–Zn–Ca alloys, Ca promotes the formation of thermally stable Mg–Zn–Ca ternary phases, enhancing the high-temperature creep resistance [15]. Ca can reduce the surface tension of the melt, improve casting fluidity, and minimize defects such as gas pores and shrinkage porosities. Regarding the improvement of fluidity, Zhao *et al.* [14] and You [16] observed that the addition of Ca reduces the atomic diffusion capability, increases melt viscosity, and consequently decreases fluidity of Mg alloys. However, the specific mechanism by which Ca influences the fluidity of magnesium alloy melts remains unclear. For viscosity, a core factor affecting melt fluidity, measurement techniques such as capillary, rotational, parallel-plate, falling-ball, and oscillating methods are available [17]. Nevertheless, the high oxidation tendency and volatility of magnesium alloy melts make it difficult to accurately determine their viscosity and structural characteristics under experimental conditions.

Molecular dynamics (MD) simulation, an atomic-scale computational method capable of accurately characterizing melt microstructures [18,19], has emerged as one of the dominant approaches for investigating melt microstructure. For instance, Xiao *et al.* [17] employed MD simulations to reveal significant short-range order structures in pure magnesium melts and found that the relationship between the self-diffusion coefficient and temperature follows the Arrhenius equation. Wang *et al.* [15] utilized *ab initio* MD simulations to study the evolution of the melt structure with composition in Mg–Al alloys at 973 K, providing new insights into the correlation between the liquid structure of Mg–Al alloys and the formation of complex solid intermetallic compounds. You *et al.* [20] employed *ab initio* MD simulations to elucidate the evolution of the melt structure with the Ca/Al ratio in Mg–Al–Ca alloys and its structural similarity to solid Laves phases. Sun *et al.* [21] applied MD simulations and the capillary fluctuation method to investigate the crystal-melt interfacial free energy of magnesium, analyzing related properties and discussing its influence on dendrite growth orientation. Zhao *et al.* [14] combined MD simulations and experimental analysis to study the effects of alloy composition on atomic diffusion and short- to medium-range order structures. Fahs *et al.* [22] performed MD simulations on the Al-rich Al–Mg–Si ternary system and its binary counterparts in the liquid and undercooled states, revealing the influence of the local structure on atomic mobility.

However, existing research on the Mg–Ca alloy system primarily focuses on the correlation between the microstructure, mechanical properties, and kinetic properties of the melt structure and diffusion. Studies investigating the viscosity-structure relationship in Mg–Ca alloys remain relatively scarce. Furthermore, conventional experimental techniques cannot directly observe microstructural evolution, necessitating complementary atomic-scale analysis via MD simulations.

Based on this, the present work employs molecular dynamics simulations (using LAMMPS) coupled with visualization software (OVITO, VMD) to investigate the influence of varying Ca content (0.1–10 wt%) on the structural parameters of magnesium alloy melts (pair distribution function, radial distribution function, coordination number, and mean squared displacement). Both equilibrium molecular dynamics (EMD) and nonequilibrium molecular dynamics (NEMD) methods are utilized to calculate the melt viscosity. The objective is to reveal the synergistic evolution mechanism of Ca content on the melt structure, viscosity, and atomic diffusion capability, thereby establishing quantitative relationships between Ca content, melt structure, and viscosity. This study aims to provide a theoretical basis for optimizing the casting process and compositional design of magnesium alloys.

2 Simulation methods

2.1 Simulated alloy systems

According to the Mg–Ca phase diagram [23], the eutectic point between magnesium and calcium corresponds to a Ca content of 10.5 wt%. Since magnesium alloy melts exist as a single phase in both the pure metal state and at the eutectic composition, where they exhibit superior fluidity, the Ca content gradients selected for this study are 0.1, 0.5, 1, 1.5, 2, 2.5, 3, 3.5, 4, 6, 8, and 10 wt%. This selection is designed to comprehensively cover the compositional range from low Ca concentrations to near-eutectic compositions, ensuring the systematic nature and representativeness of the research findings.

2.2 Melt structural parameters

This study characterizes the structural information of the melt through MD calculations of the pair distribution function, radial distribution function, coordination number, Voronoi index, and H–A index (i.e., Honeycutt–Anderson bond pair index). The definitions and calculation methods for each parameter are as follows.

The pair distribution function (PDF) is used to reveal the atomic distribution characteristics of the Mg–Ca melt at 1000 K. The PDF provides a statistical analysis of the overall structural features and reflects the ensemble average of the structural information. The pair distribution function is defined as Eq. (1) [24]:

$$g(r) = \frac{1}{\rho 4\pi r^2} \frac{\sum_{i=1}^{T} \sum_{j=1}^{N} \Delta N(r \to r + \delta_r)}{N \times T} \tag{1}$$

where N is the number of atoms, T is the total time step, δ_r is the prescribed distance interval, ΔN denotes the number of atoms located between distances r and $r + \delta_r$, and ρ is the atomic number density.

The radial distribution function (RDF) represents the average number of atoms within a spherical shell of radius r surrounding a central atom. Its value equals the product of the particle probability density at that position and the surface area of the spherical shell, defined as Eq. (2) [25]:

$$G(r) = 4\pi r^2 \left(\frac{N}{V}\right) g(r) = 4\pi r^2 \rho g(r) \tag{2}$$

where V is the volume of the simulation system, and the meanings of the remaining parameters are consistent with those in Eq. (1).

The coordination number characterizes the number of nearest

neighboring atoms directly adjacent to a central atom, reflecting the bonding capacity and coordination relationship between the central atom and its surroundings. It is calculated by integrating the first peak of the RDF, expressed as Eq. (3)[25]:

$$Z = \int_0^{r_{\min}} g(r)\, 4\pi\rho r^2 \mathrm{d}r \tag{3}$$

where Z is the coordination number, and the upper integration limit ($r_{\min}$) corresponds to the position of the first minimum after the first peak in the radial distribution function, i.e., the maximum distance of the first nearest neighbor atoms.

Voronoi polyhedron analysis characterizes the topological features of melt configurations by constructing Voronoi polyhedra that enclose atoms, partitioning the three-dimensional space into atomic coordination cells [24]. Different Voronoi polyhedra are described using the Voronoi index $<n_3, n_4, n_5, n_6>$, where n_i represents the number of i-edged faces on the surface of the Voronoi polyhedron. This index clearly reflects the arrangement characteristics of neighboring atoms surrounding the central atom.

Honeycutt–Anderson analysis (H–A analysis, common neighbor analysis) investigates local atomic configurations in liquid systems. According to the H–A scheme [16,26], the indices i, j, k, and l characterize bonding pairs of atoms and their common neighbors, precisely describing the local bonding environment and providing crucial insights into the degree of ordering in atomic arrangements within the melt.

2.3 Self-diffusion coefficient

The calculation of the diffusion coefficient in an alloy system requires prior determination of the mean squared displacement (MSD). The MSD represents the average of the squared particle displacements over a given time interval, quantifying the average distance of particle motion and reflecting the extent of particle diffusion or disorder [17]. It is expressed as Eq. (4):

$$\mathrm{MSD}(t) = \frac{1}{N}\sum_{i=1}^{N}\left\langle [r_i(t+\tau) - r_j(\tau)]^2 \right\rangle \tag{4}$$

where N is the total number of atoms in the system, $r_i(\tau)$ is the position vector of atom i at time τ, and $< \ldots >$ denotes the ensemble average.

When the data sampling time is sufficiently long, the MSD exhibits a linear relationship with the self-diffusion coefficient (D), as described by the Stokes–Einstein equation, from which the self-diffusion coefficient can be calculated (Eq. (5)):

$$D_{\mathrm{MSD}} = \frac{1}{6}\lim_{t\to 0}\frac{\mathrm{MSD}(t)}{t} \tag{5}$$

2.4 Viscosity

In MD simulations, the viscosity is commonly calculated using two methods: the equilibrium method based on the stress autocorrelation function and the nonequilibrium method based on the velocity autocorrelation function. This study employs both methods to calculate the melt viscosity, ensuring the accuracy of the viscosity data.

1) Equilibrium molecular dynamics (EMD) method

This method is suitable for thermodynamic equilibrium systems. By statistically analyzing the potential energy, kinetic energy, and stress tensor of each particle, the temporal evolution of the stress autocorrelation function is obtained. After a sufficiently long simulation time, the stress autocorrelation function converges to a constant value. The viscosity is then obtained by integrating the stress autocorrelation function over time using the Green–Kubo relation. Notably, the viscosity calculation based on the stress autocorrelation function is highly sensitive to time. Therefore, a sufficiently long simulation time is required to ensure that the correlation function converges to an equilibrium state to avoid computational errors.

2) Nonequilibrium molecular dynamics (NEMD) method

This study employs the Müller–Plathe method to calculate the viscosity of liquid metals. The core principle involves measuring the velocity gradient generated after momentum exchange by simulating momentum transfer between the central and bottom regions of the system. The viscosity is calculated as the ratio of the total momentum flux transferred to the resulting velocity gradient. During the calculation, the frequency of momentum exchange is a critical parameter: if the momentum exchange is too small, the velocity gradient can maintain a linear response regime, and errors can be corrected via linear regression [27]; if the momentum exchange is too large, the momentum transfer loses uniformity, leading to a significant increase in simulation error [23].

2.5 Simulation procedure

The MD simulations employed the modified embedded-atom method (MEAM) potential developed by Kim *et al.* [28]. This potential has been extensively validated by numerous studies to accurately describe the physical properties and microstructure of the Mg–Ca system [29,30], ensuring the reliability of the simulation results.

The initial configuration is a hexagonal close-packed (HCP) crystal, with lattice vectors constructed using custom parameters (a = 3.2 Å, c/a = 1.6235). The simulation box is a cube with a side length of 20 unit cells. Periodic boundary conditions are applied throughout the simulation. The Newtonian equations of motion are integrated using the Verlet leapfrog algorithm within the NVE ensemble (constant number of particles, volume, and energy), with an integration time step of 1 fs.

The solidification simulation process is divided into two stages: heating/relaxation and cooling.

1) Heating and relaxation stage: The initial model is heated to 1300 K within the isothermal-isobaric (NPT) ensemble (constant number of particles, pressure, and temperature) and relaxed for 1,000,000 steps. This ensures complete melting of the alloy system and eliminates the influence of the initial crystal structure on subsequent simulations.

2) Cooling stage: The fully molten alloy system is cooled from 1300 to 1000 K at a rate of 1×10^{12} K/s, with a cooling time step of 0.001 ps, yielding the data files for the melting and solidification process.

Based on the solidification data, the system is placed in the NPT ensemble and fully relaxed for 500,000 steps with a time step of 0.001 ps to ensure that the system reaches thermodynamic equilibrium. After relaxation, the structural parameters and dynamic property parameters of Mg–Ca melts with different Ca contents are calculated using the methods described above.

3 Results and discussion

3.1 Structural characteristics of magnesium alloy melts

3.1.1 Pair distribution function

The PDF describes the probability of finding other particles at a radius r from an arbitrarily specified central particle. Figure 1 shows the PDF curves for Mg–Ca alloy melts with different Ca contents at 1000 K, where Fig. 1(a) presents the total PDF curves

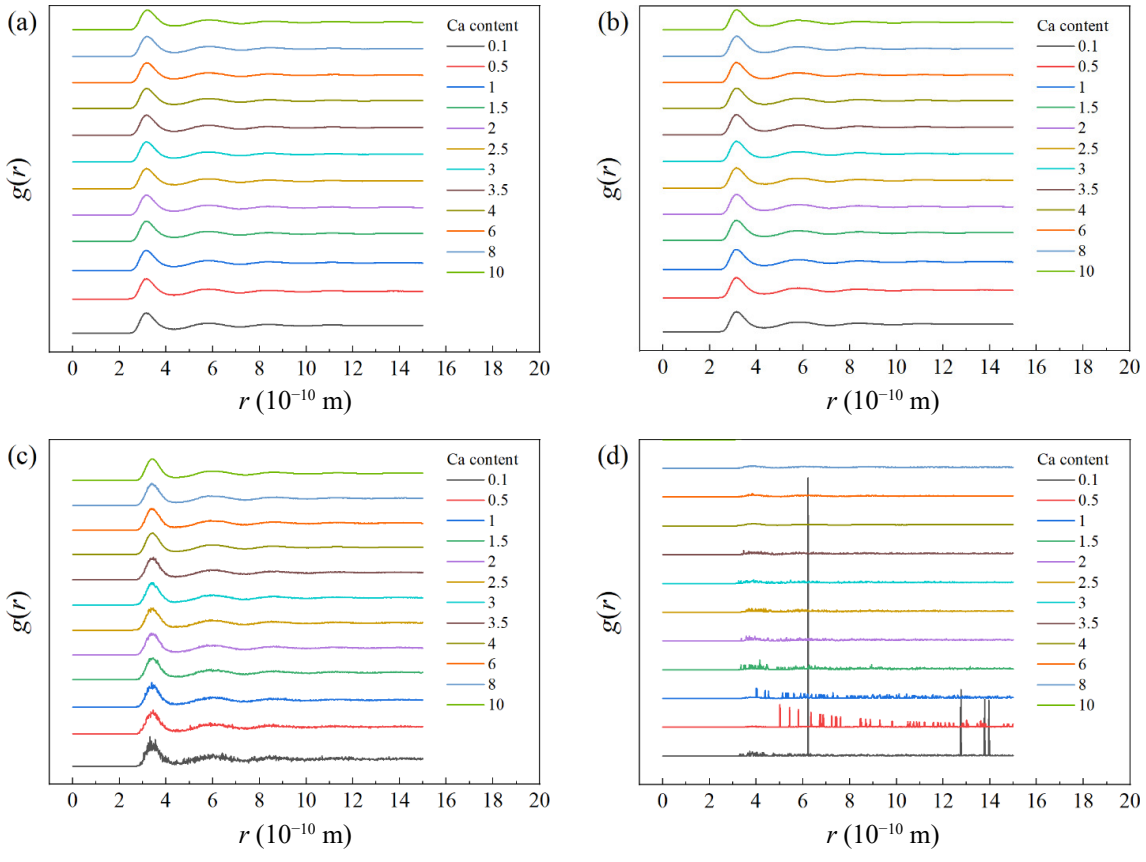

Fig. 1 Total and partial PDFs of liquid Mg–Ca alloys with different Ca contents studied at 1000 K, including (a) Total PDF $g_{Total}(r)$, (b) Mg–Mg partial PDF $g_{Mg-Mg}(r)$, (c) Mg–Ca partial PDF $g_{Mg-Ca}(r)$, (d) Ca–Ca partial PDF $g_{Ca-Ca}(r)$.

for the Mg–Ca alloys; Fig. 1(b) displays the partial PDF curves for Mg–Mg atomic pairs; Fig. 1(c) illustrates the partial PDF curves for Mg–Ca atomic pairs; Fig. 1(d) depicts the PDF curves for Ca–Ca atomic pairs. Common characteristics observed in the PDF curves include the following: all curves exhibit a relatively high first peak, only three peaks appear within the 0–10 Å range, and the PDF value converges to 1 as the radius r increases. This phenomenon indicates that at a temperature of 1000 K, the Mg–Ca alloy systems with Ca contents ranging from 0.1 to 10 wt% all exist in a typical liquid state characterized by short-range order and long-range disorder, consistent with the structural features of liquid metals.

3.1.2 *Coordination number*

The coordination number represents the number of atoms surrounding a given central atom. The partial coordination number (Z_{ij}) denotes the number of j atoms located within the first coordination shell of an i atom. The distance defining the first coordination shell is determined by the position of the first minimum after the first peak in the radial distribution function. The partial coordination number is obtained by integrating the first peak of the corresponding partial radial distribution function. The total coordination number is equal to the sum of all relevant partial coordination numbers, for example, $Z_{Mg} = Z_{Mg-Mg} + Z_{Mg-Ca}$.

Table 1 records the calculated partial and total coordination numbers for liquid Mg–Ca alloy systems with different Ca contents at 1000 K. As the Ca content increases, the partial coordination numbers for both Mg and Ca atoms exhibit minor fluctuations (e.g., Z_{Mg-Mg} decreases from 11.806 at 0.1 wt% Ca to 11.453 at 2.5 wt% Ca and then increases to 11.655 at 3 wt% Ca), while the total coordination number remains largely stable (e.g., $Z_{Mg-total}$ ranges from 11.418 to 11.890 and $Z_{Ca-total}$ ranges from 12.471 to 13.699). This demonstrates that the increase in Ca content has a limited effect on the atomic coordination numbers in the Mg–Ca alloy melt, indicating that the atomic packing mode remains largely unchanged and that the melt structure exhibits high stability at the atomic coordination level.

3.1.3 *Voronoi index*

This study extracted Voronoi indices corresponding to Voronoi polyhedra with an area fraction exceeding 1% and selected the five most representative indices (<0,3,6,4>, <0,2,6,4>, <0,1,10,2>, <0,1,8,4>, <0,2,8,2>) to characterize the local short-range topological order of the melt structure. Figure 2(a) shows the distribution of Voronoi indices in Mg–Ca alloy systems with different Ca contents, while Fig. 2(b) illustrates the variation in the population fraction of these selected Voronoi indices with increasing Ca content. The Voronoi indices in the Mg–Ca alloy melts exhibit oscillatory changes with increasing Ca content, although the overall variation is modest (e.g., the fraction of <0,3,6,4> ranges from ~0.019 to ~0.021), indicating no fundamental transformation in the local melt structure. Further analysis shows that the variation in Voronoi indices is more pronounced in the low Ca content range (< 4 wt%) than in the medium-high Ca content range (≥ 4 wt%). This phenomenon suggests that Ca atoms induce more significant perturbations to the local melt structure at lower concentrations. When the Ca content increases to a certain level (≥ 4 wt%), the local melt structure gradually stabilizes and becomes less sensitive to further Ca additions.

3.1.4 H–A Index

Figures 3(a) and 3(b) show the percentage of typical H–A bond pairs and the corresponding proportion of local ordered structures, respectively, in liquid Mg–Ca alloy systems with different Ca contents at 1000 K. In the 0.1–4 wt% Ca range, the proportions of bond pairs 1441, 1541, 1551, and 1661 generally increase first and then decrease, while those of bond pairs 1311, 1321, 1421, 1422, and 1431 decrease first and then increase. At 1.5 wt% Ca, the variation in bond pair percentages deviates from the aforementioned trend, showing an abnormal decrease or increase, which is attributed to transient local structural reorganization at this specific composition. When the Ca content ranges from 4 to 10 wt%, the percentages of all bond pairs remain essentially stable with increasing Ca content, indicating that the melt structure has stabilized and is less sensitive to Ca content variation.

Table 1 Partial coordination numbers, total coordination numbers of Mg atoms and Ca atoms in Mg–Ca alloys with different Ca contents at 1000 K

Ca content (wt%)	Partial coordination number				Total coordination number	
	Z_{Mg-Mg}	Z_{Mg-Ca}	Z_{Ca-Mg}	Z_{Ca-Ca}	$Z_{Mg-total}$	$Z_{Ca-total}$
0.1	11.806	0.008	12.835	—	11.813	12.835
0.5	11.713	0.041	13.699	—	11.754	13.699
1.0	11.602	0.080	13.186	0.067	11.682	13.200
1.5	11.540	0.120	13.144	0.137	11.660	13.281
2.0	11.553	0.151	12.316	0.155	11.704	12.471
2.5	11.453	0.192	12.490	0.198	11.645	12.688
3.0	11.655	0.235	12.679	0.225	11.890	12.904
3.5	11.456	0.275	12.656	0.261	11.731	12.917
4.0	11.408	0.314	12.548	0.330	11.722	12.878
6.0	10.963	0.460	12.003	0.535	11.423	12.538
8.0	10.797	0.621	11.901	0.630	11.418	12.531
10.0	10.837	0.804	12.067	0.825	11.641	12.892

Note: "—" indicates that no Ca–Ca atomic coordination relationship is detected at this Ca content.

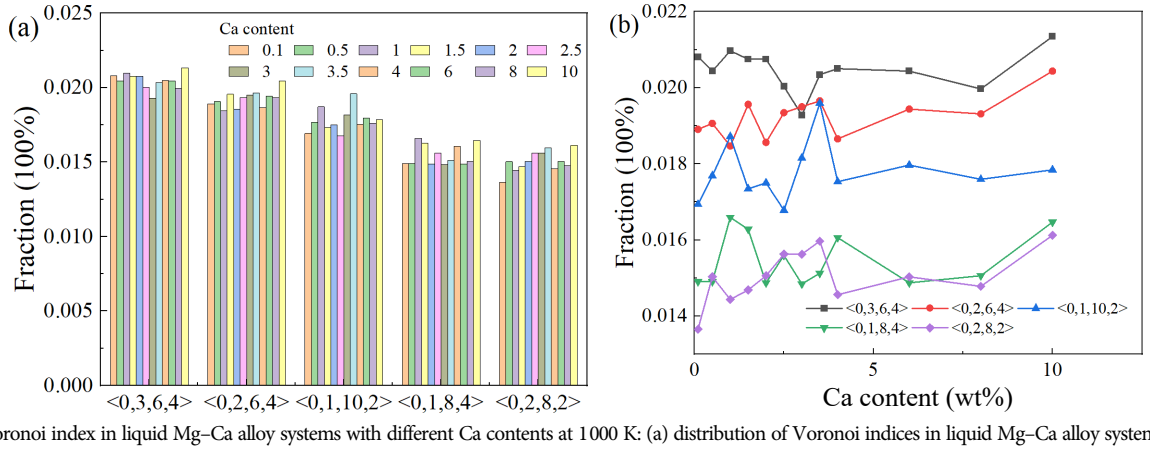

Fig. 2 Voronoi index in liquid Mg–Ca alloy systems with different Ca contents at 1000 K: (a) distribution of Voronoi indices in liquid Mg–Ca alloy systems with Ca contents of 0.1, 0.5, 1, 1.5, 2, 2.5, 3, 3.5, 4, 6, 8, 10 wt%; (b) variation of each Voronoi index with increasing Ca content.

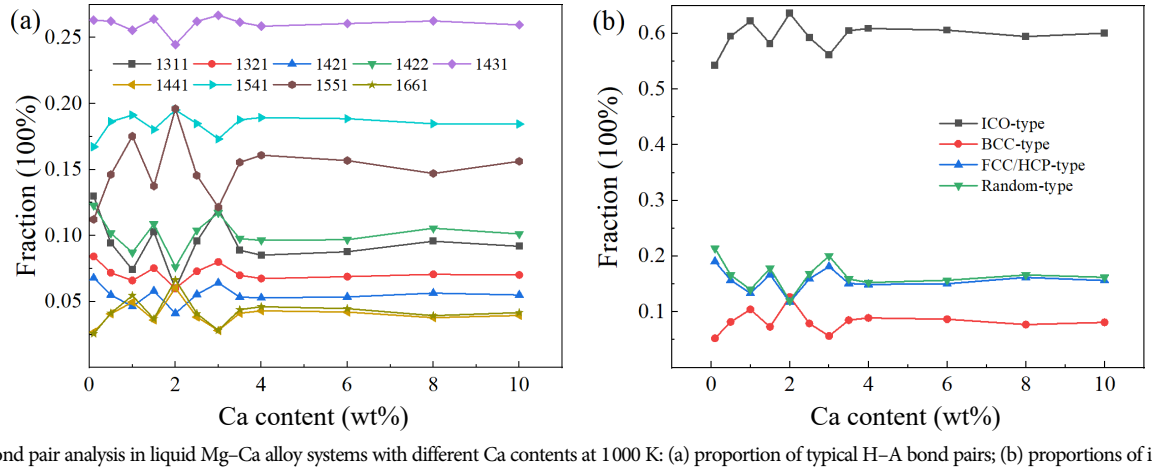

Fig. 3 Bond pair analysis in liquid Mg–Ca alloy systems with different Ca contents at 1000 K: (a) proportion of typical H–A bond pairs; (b) proportions of icosahedral (ICO)-type (1551, 1541, and 1431), body-centered cubic (BCC)-type (1441 and 1661), face-centered cubic/hexagonal close-packed (FCC/HCP)-type (1421 and 1422), and random-type structures.

In Fig. 3(b), the proportions of ICO-type (icosahedral), BCC-type (body-centered cubic), FCC/HCP-type (face-centered cubic/hexagonal close-packed), and random-type bond pairs all undergo noticeable changes in the 0.1–4 wt% Ca range. The proportions of ICO-type and BCC-type bond pairs increase first and then decrease, while those of FCC/HCP-type bond pairs decrease first and then increase. When the Ca content is between 4 and 10 wt%, all bond pair types remain nearly constant, with ICO-type bond pairs consistently predominant, accounting for the largest proportion of the local ordered structure. These results further confirm that the structure of the Mg–Ca alloy melt is significantly influenced by Ca content and exhibits poorer stability at low Ca concentrations, whereas the structural stability is markedly enhanced at high Ca concentrations. Additionally, ICO-type bond pairs are identified as the primary factor maintaining the short-range ordered structure of the alloy melt.

3.2 Diffusion behavior

Figure 4 shows the relationship between the mean squared displacement (MSD) and time for Mg–Ca alloy melts with different Ca contents at 1000 K. Table 2 presents the slopes of the MSD-time curves and the corresponding atomic self-diffusion coefficients for Mg and Ca atoms at 1000 K. The MSD is calculated by summing the squared displacements of atoms within the simulated system along the *x*, *y*, and *z* directions. Its evolution with time directly reflects the rate of atomic diffusion. The MSD of both Mg and Ca atoms increases linearly with time, consistent with the diffusive behavior of liquid metals. At the same time, the MSD value decreases with increasing Ca content, indicating reduced atomic mobility.

Combining the data from Fig. 4 and the slope values for Mg atoms in Table 2, it is evident that the atomic diffusion behavior in Mg–Ca alloy melts exhibits a distinct concentration dependence. In the low Ca content range (0.1–2.5 wt%), the diffusion capabilities of both Mg and Ca atoms exhibit fluctuating changes with increasing Ca content, without displaying a clear monotonic trend, e.g., the Mg self-diffusion coefficient fluctuates between 0.5726×10^{-9} and 0.6121×10^{-9} m²/s, and the Ca self-diffusion coefficient fluctuates between 0.3733×10^{-9} and 0.4047×10^{-9} m²/s. This is attributed to Ca atoms acting as "impurity atoms" that cause minor perturbations to the melt structure, coupled with the possible presence of local atomic vacancies or defects. Upon entering the high calcium content range (≥ 3 wt%), the diffusion capabilities of both atoms gradually decrease with increasing Ca content, e.g., the Mg self-diffusion coefficient decreases from 0.5775×10^{-9} to 0.5064×10^{-9} m²/s when the Ca content changes from 3 to 10 wt%. This phenomenon can be attributed to the enhanced interatomic interactions within the system at high Ca contents, which increases the resistance to atomic motion and consequently reduces the diffusion capability.

3.3 Viscosity

Figure 5 shows the relationship between the viscosity of Mg–Ca alloy melts and the Ca content at 1000 K, with curves calculated

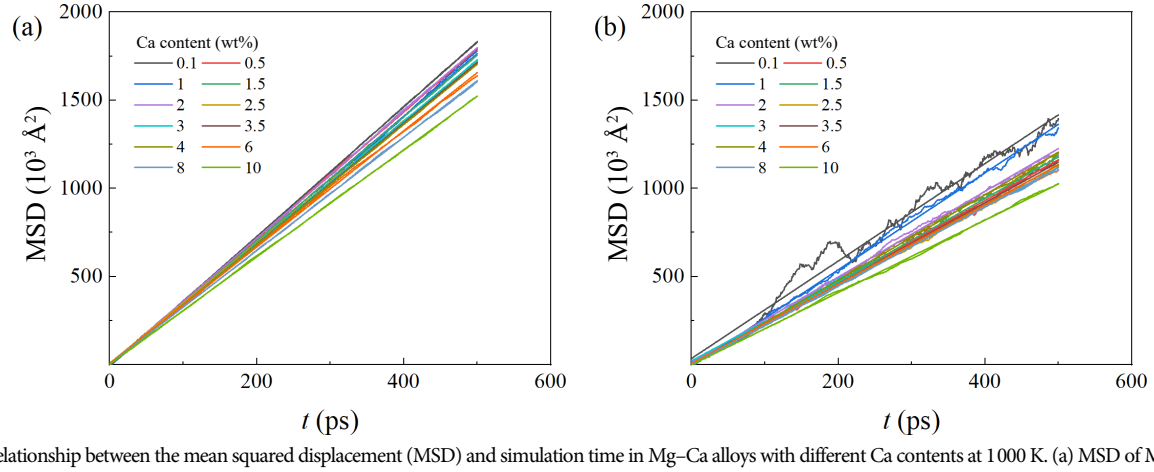

Fig. 4 Relationship between the mean squared displacement (MSD) and simulation time in Mg–Ca alloys with different Ca contents at 1000 K. (a) MSD of Mg atom in Mg–Ca alloys with different Ca contents; (b) MSD of Ca atom in Mg–Ca alloys with different Ca contents.

Table 2 Slopes of the mean squared displacement (MSD) vs time curves for Mg atoms and Ca atoms and diffusion coefficients of Mg atoms and Ca atoms in Mg–Ca alloy melts with different Ca contents at 1000 K

Ca content (wt%)	Mg MSD slope (10^{-9} m²/s)	Ca MSD slope (10^{-9} m²/s)	Mg self-diffusion coefficient (10^{-9} m²/s)	Ca self-diffusion coefficient (10^{-9} m²/s)
0.1	3.6727	2.7644	0.6121	0.4607
0.5	3.5909	2.3241	0.5985	0.3874
1.0	3.5456	2.7482	0.5909	0.4580
1.5	3.5127	2.3594	0.5855	0.3932
2.0	3.6020	2.4282	0.6003	0.4047
2.5	3.4357	2.2398	0.5726	0.3733
3.0	3.4651	2.2173	0.5775	0.3696
3.5	3.4368	2.3007	0.5728	0.3834
4.0	3.4088	2.4171	0.5681	0.4028
6.0	3.2959	2.2539	0.5493	0.3757
8.0	3.2130	2.2361	0.5355	0.3727
10.0	3.0387	2.0533	0.5064	0.3422

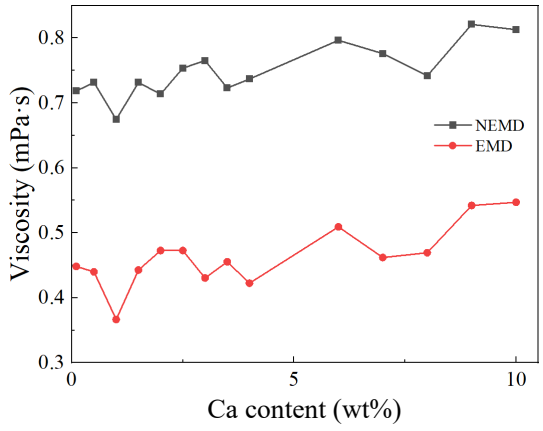

Fig. 5 Curves of the viscosity of Mg–Ca alloy melts with different Ca contents at 1000 K.

by the EMD and NEMD methods. The melt viscosity exhibits an overall increasing trend with increasing Ca content, albeit with local fluctuations. This aligns with decreasing atomic diffusion capability, i.e., higher viscosity corresponds to greater resistance to atomic motion. At 1 wt% Ca, the melt viscosity is lower than that at 0.1 wt%, indicating that the addition of calcium at this specific concentration reduces the viscosity of the magnesium alloy melt. This observation corresponds to the fluctuating characteristics of the melt structure at low Ca contents. Within the Ca content range of 0.1–4 wt%, the variation in viscosity with increasing Ca content is relatively complex, consistent with the oscillatory trends described previously for the melt structure (e.g., H–A index, Voronoi index). Furthermore, distinct inflection points in viscosity occur at 1, 6, and 8 wt% Ca, which are speculated to correspond to local structural reorganization or significant changes in the degree of order within the melt.

The variation trend of viscosity calculated by the equilibrium method is consistent with that obtained by the nonequilibrium method. This agreement verifies the reliability of the viscosity data and confirms that the Ca content influences the viscosity of Mg–Ca alloy melts in a predictable pattern, closely correlated with the melt structure evolution.

3.4 Correlation between melt structure and viscosity

Integrating the aforementioned results, the degree of structural order, Voronoi indices, and proportion of ICO-type bond pairs in Mg–Ca alloy melts exhibit similar trends. The changes in both melt viscosity and atomic diffusion capability show significant correlations with the evolution of the melt structure, which can be specifically described in the following two aspects:

The pair distribution function curves reveal that the variation in the height of the first peak (a key indicator of short-range order) correlates strongly with viscosity. A higher first peak signifies greater short-range order, which increases resistance to atomic motion and thus raises viscosity. This confirms a strong positive correlation between melt order and viscosity.

From the perspective of the characteristics of the Voronoi and H–A indices, the proportions of various bond pair types and the Voronoi indices fluctuate markedly with increasing Ca content within the low Ca range (< 4 wt%). This indicates significant structural fluctuations within the melt. Consequently, the melt viscosity is influenced jointly by the types of bond pairs (e.g., the proportions of ICO-type and BCC-type pairs) and the local spatial configurations of the melt (characterized by Voronoi indices), leading to complex fluctuations superimposed on an overall increasing trend.

The atomic radius of Ca (1.97 Å) is larger than that of Mg (1.60 Å). At low Ca contents (< 4 wt%), the Ca atoms are embedded in the Mg atomic lattice as "impurities", disrupting the local coordination balance and leading to frequent transitions of the Voronoi index (e.g., alternating fluctuations in the proportions of <0,3,6,4> and <0,2,6,4>). The Ca atoms can form strong bonds with surrounding Mg atoms, temporarily forming local atomic clusters. The formation and dissociation of these clusters cause fluctuations in the proportion of H–A bond pairs (e.g., the remarkable decrease in type 1551 bond pairs at 1.5 wt% Ca).

Upon entering the high Ca range (≥ 4 wt%), the proportions of the bond pairs stabilize, e.g., ICO-type pairs remain dominant, and the melt structure becomes more stable. Additionally, the variation in Voronoi indices with Ca content aligns closely with the trend in viscosity change. This suggests that within this range, the change in melt viscosity is primarily governed by the evolution of the local spatial configuration of the melt (Voronoi indices), showing a steadily increasing trend with increasing Ca content.

The three viscosity inflection points at 1, 6, and 8 wt% Ca can be directly mapped to the melt structural parameters. In detail, the proportions of FCC/HCP-type and random-type bond pairs decrease from 0.16 and 0.17 at 0.5 wt% Ca to 0.13 and 0.14 at 1 wt% Ca, respectively, and the proportion of the Voronoi index <0,2,6,4> decreases to 0.018, corresponding to a local decrease in viscosity. In addition, the position of the first peak in the total PDF $g_{Total}(r)$ shifts from 3.18 Å at 0.5 wt% Ca to 3.12 Å at 1 wt% Ca, and $Z_{Mg-total}$ decreases to 11.682 (a decrease of 0.072 compared to 0.5 wt% Ca), indicating the contraction of the Mg atomic coordination shell and local structural loosening, further corresponding to the decrease in viscosity. At 6 wt% Ca, the proportion of ICO-type bond pairs maintains a high value (0.61), and the proportion of the Voronoi index <0,2,8,2> increases to 0.015. The improved structural order leads to a significant increase in viscosity. At 8 wt% Ca, the proportion of the Voronoi index <0,1,8,4> changes abruptly, and the proportion of ICO-type bond pairs decreases to 0.59, changing structural rigidity, which corresponds to the viscosity inflection point at this Ca content.

The correlation mechanism provides clear guidance for optimizing the viscosity of Mg–Ca alloy melts by controlling the Ca content. In the low Ca content range, the viscosity can be reduced, and the fluidity is improved by precisely controlling the Ca content (e.g., approximately 1 wt%). In the high Ca content range, the focus should be placed on monitoring the local spatial configuration of the melt to achieve precise control of viscosity through compositional adjustments.

3.5 Effect of temperature fluctuations

In practical casting processes, temperature fluctuations are inherent and unavoidable. Specifically, the temperature fluctuations around the studied 1000 K may directly alter the thermal kinetic energy of melt atoms: a slight increase in temperature could enhance atomic diffusion (increasing the diffusion coefficient), weaken the stability of local atomic clusters (e.g., reducing the proportion of ICO-type bond pairs), and thereby lower the melt viscosity. Conversely, a moderate temperature decrease may promote the ordering of the melt structure (e.g., increasing the proportion of FCC/HCP-type bond pairs) and elevate viscosity. Such viscosity variations, in turn, can affect key casting processes. For instance, higher viscosity may impede melt flowability during mold filling, while lower viscosity might increase the risk of shrinkage defects during solidification.

4 Conclusions

This study employed molecular dynamics simulations to calculate

the structural parameters (pair distribution function, coordination number, Voronoi index, H–A index) and dynamic property parameters (diffusion coefficient, viscosity) of Mg–Ca alloy systems with Ca contents ranging from 0.1 to 10 wt% at 1000 K. Through systematic analysis of the simulation results, the following main conclusions are drawn:

1) At 1000 K, all Mg–Ca alloy systems exhibit liquid-state structural characteristics, namely, long-range disorder and short-range order, with ICO-type bond pairs remaining predominant across the entire Ca content range. The variation trends of the structural order, the proportion of ICO-type bond pairs, and the Voronoi indices with increasing Ca content are highly consistent. At low Ca concentrations (< 4 wt%), all three parameters exhibit significant fluctuations, e.g., the proportions of ICO-type bond pairs increase first and then decrease, indicating poor structural stability of the melt. At high Ca concentrations (≥ 4 wt%), the structural order increases slightly with Ca content, the proportion of the ICO-type bond pairs stabilizes, and the Voronoi indices show a mild increasing trend, markedly enhancing the structural stability.

2) The viscosity of Mg–Ca alloy melts generally shows an increasing trend with increasing Ca content, with values confirmed by both EMD and NEMD methods. The inflection points occur at 1, 6, and 8 wt% Ca, corresponding to local structural reorganization. These specific composition points (e.g., 1 wt% Ca) represent potential compositional windows for improving melt fluidity by reducing viscosity.

3) The changes in viscosity and atomic diffusion capability are highly correlated with the evolution of the melt structure in Mg–Ca alloy melts. At low Ca concentrations (< 4 wt%), the melt structure fluctuates significantly, and the viscosity exhibits an overall increasing trend with superimposed oscillations, consistent with structural variations. At high Ca concentrations (≥ 4 wt%), the types of bond pairs stabilize, and the change in viscosity is primarily governed by the evolution of the local spatial configuration of the melt, showing a steady increase with Ca content.

By establishing quantitative relationships and correlation mechanisms between Ca content, melt structure, and viscosity, this study provides important theoretical support for the compositional design and casting process optimization of Mg–Ca alloys. It also offers a referential methodology and perspective for research on the melt structure and viscosity of other Mg alloy systems.

The current study is limited to a single temperature of 1000 K and does not explore the synergistic effect of temperature and Ca content on the melt structure–viscosity relationship. As discussed in Section 3.5, the temperature is a key variable in the actual casting process. Meanwhile, the study simplifies the industrially commonly used Mg–Ca–X (e.g., X = Zn, Al) multicomponent alloy systems to binary alloys, which limits the industrial applicability of the research conclusions. Future studies can focus on simulations at multiple temperatures and research on multicomponent systems to improve the theoretical framework and enhance application value. Through elucidating the coupling law of temperature–Ca content and the regulatory mechanism of elements such as Zn and Al, a more comprehensive structure–viscosity regulation map can be established, which can promote the transformation of research conclusions to industrial practical applications.

Acknowledgements

This work is financially supported by the National Natural Science Foundation of China (No. 52471118), the Advanced Materials-National Science and Technology Major Project (No. 2024ZD0601400), the New Chongqing Youth Innovation Talent Project (No. CSTB2025YITP-QCRCX0043), the State Key Laboratory of Solidification Processing in NPU (No. SKLSP202521), and the Young Elite Scientists Sponsorship Program by CAST (No. 2022QNRC001).

Author contributions

Dengyuan Qi: Conceptualization, Methodology, Validation, Writing – original draft. Ang Zhang: Conceptualization, Methodology, Writing – original draft, Writing – review & editing, Funding. Lijun Zhang: Methodology, Investigation, Validation. Tao Jiang: Methodology, Investigation. Feng He: Methodology and conceptualization. Jun Wang: Methodology, conceptualization. Zehua Li: Investigation. Xiao Li: Investigation. Jiangfeng Song: Methodology, Investigation. Bin Jiang: Investigation, Funding.

Availability of data and materials

The data that support the findings of this study are available from the corresponding author upon reasonable request.

Competing interests

The authors declare that they have no known competing financial interests or personal relationships that could have appeared to influence the work reported in this paper.

References

[1] Wu XY. Present situation and development countermeasures of exploitation and utilization of magnesium resources in China. *Modern Ming* 2023, **39**: 33–38, 48. (in Chinese)

[2] Chen WT, Yang JY, Yu WB, *et al.* One developed finite element model used in nano-layered flaky Ti_2AlC MAX ceramic particles reinforced magnesium composite. *J Magnes Alloys* 2024, **12**: 4219–4228.

[3] Li T, Song JF, Zhang A, *et al.* Progress and prospects in Mg-alloy super-sized high pressure die casting for automotive structural components. *J Magnes Alloys* 2023, **11**: 4166–4180.

[4] Li YF, Zhang A, Li CM, *et al.* Recent advances of high strength Mg–RE alloys: Alloy development, forming and application. *J Mater Res Technol* 2023, **26**: 2919–2940.

[5] Ma XJ, Lin CH, Yang HY, *et al.* Elevating thermoelectric performance in the sub-ambient temperature range for electronic refrigeration. *Innovation* 2025, **6**: 100864.

[6] Jiang B, Dong ZH, Zhang A, *et al.* Recent advances in micro-alloyed wrought magnesium alloys: Theory and design. *Trans Nonferrous Met Soc China* 2022, **32**: 1741–1780.

[7] Cao FH. Evaluation of microstructrue and mechanical property of Mg alloys during close-die hot-pressing of extruded preforms. Ph.D. Thesis. China: Chongqing University, 2010. (in Chinese)

[8] Mi HH, Yang Y, Fu RH, *et al.* Synergistically regulating the mechanical properties and damping capacity of Mg–6Gd–5Y–1Zn–0.4Zr ring prepared by centrifugal casting. *J Alloys Compd* 2025, **1035**: 181555.

[9] Chen HX, Zhang A, Li H, *et al.* Segregation of Mg–6Gd alloy under natural convection: From macro solute distribution to micro dendrite growth. *China Foundry* 2024, **21**: 613–624.

[10] Yang MH, Zhang A, Qin L, *et al.* Morphological evolution of Mg–Gd dendrite array: A numerical investigation extended from *in situ* X-ray radiography. *Trans Mater Res* 2025, **1**: 100115.

[11] Wen LH, Ji ZS. Research and application of heat-resistant magnesium alloy and its strengthening mechanism. *Light Alloy Fabr Technol* 2014, **42**: 28–34, 50. (in Chinese)

[12] Liu SY, Apell J, Liu ZH, *et al.* Raising the oxidation resistance of low-

alloyed Mg–Ca alloys through a preheating treatment in an argon atmosphere. *Materials* 2024, **17**: 5481.
[13] Zheng J. Study on the calcium magnesium alloy mechanical properties and corrosion behavior. Ph.D. Thesis. China: Chang'an University, 2015. (in Chinese)
[14] Zhao YF, Lin DY, Chen XH, *et al*. Sluggish mobility and strong icosahedral ordering in Mg–Zn–Ca liquid and glassy alloys. *Acta Mater* 2014, **67**: 266–277.
[15] Wang J, Li XX, Pan SP, *et al*. Mg fragments and Al bonded networks in liquid Mg–Al alloys. *Comput Mater Sci* 2017, **129**: 115–122.
[16] You J. Machine learning-driven simulation study of structure and dynamics in magnesium and aluminum alloy melts and their effects on solidification behavior. Ph.D. Thesis. China: Jilin University, 2024. (in Chinese)
[17] Xiao JJ, Zhao X, Wu YQ. Research on viscosity and self-diffusion coefficient of liquid Mg by molecular dynamics simulation. *J Anhui Univ Technol Nat Sci* 2023, **40**: 261–268. (in Chinese)
[18] Chen HC, Sun JL, Yang SL, *et al*. Thermodynamics and kinetics of isothermal precipitation in magnesium alloys. *Mater Genome Eng Adv* 2025, **3**: 86.
[19] Zhang W, Xie HC, Ma ZC, *et al*. Graphene oxide-induced substantial strengthening of high-entropy alloy revealed by micropillar compression and molecular dynamics simulation. *Research* 2022, **2022**: 9839403.
[20] You J, Wang C, Shang SL, *et al*. Ordering in liquid and its heredity impact on phase transformation of Mg–Al–Ca alloys. *J Magnes Alloys* 2023, **11**: 2006–2017.
[21] Sun DY, Mendelev MI, Becker CA, *et al*. Crystal-melt interfacial free energies in hcp metals: A molecular dynamics study of Mg. *Phys Rev B* 2006, **73**: 024116.
[22] Fahs A, Jarry P, Jakse N. Structure-dynamics relationship in Al–Mg–Si liquid alloys. *Phys Rev B* 2023, **108**: 224202.
[23] Liu CM, Zhu XR, Zhou HT. *Magnesium Alloy Phase Diagrams*. Changsha (China): Central South University Press, 2006.
[24] Cheng YQ, Ma E. Atomic-level structure and structure–property relationship in metallic glasses. *Prog Mater Sci* 2011, **56**: 379–473.
[25] Zhang SL, Qi L, Gao W, *et al*. Summary of methods for structural analysis and characterization in molecular modeling. *J Yanshan Univ* 2015, **39**: 213–220. (in Chinese)
[26] Honeycutt JD, Andersen HC. Molecular dynamics study of melting and freezing of small Lennard–Jones clusters. *J Phys Chem* 1987, **91**: 4950–4963.
[27] Luo CL, Min Y, Guo PY, *et al*. Molecular dynamics simulation of the structure and transport properties of Fe–Cr–Ni alloy melts. *J Non Cryst Solids* 2025, **650**: 123362.
[28] Kim KH, Jeon JB, Lee BJ. Modified embedded-atom method interatomic potentials for Mg–X (X = Y, Sn, Ca) binary systems. *Calphad* 2015, **48**: 27–34.
[29] Liu LJ, Miyake M, Li L, *et al*. Numerical study on the ductility improvement mechanism of dilute Mg–Ca alloys. *Comput Mater Sci* 2023, **228**: 112381.
[30] Shankar A, Bhatt NK. Enhanced mechanical and thermophysical properties of Mg_2Ca, Al_2Ca, and Al_4Ca bulk metallic glasses in comparison to crystalline alloys for bone grafting applications: A molecular dynamics investigation. *J Appl Phys* 2024, **136**: 035107.